BIOCHEMISTRY
including biophysical chemistry & molecular biology

Article

pubs.acs.org/biochemistry

Structure of a Dinuclear Iron Cluster-Containing β-Hydroxylase Active in Antibiotic Biosynthesis

Thomas M. Makris,† Cory J. Knoot, Carrie M. Wilmot,* and John D. Lipscomb*

Department of Biochemistry, Molecular Biology and Biophysics and Center for Metals in Biocatalysis, University of Minnesota, Minneapolis, Minnesota 55455, United States

Supporting Information

ABSTRACT: A family of dinuclear iron cluster-containing oxygenases that catalyze β-hydroxylation tailoring reactions in natural product biosynthesis by nonribosomal peptide synthetase (NRPS) systems was recently described [Makris, T. M., Chakrabarti, M., Münck, E., and Lipscomb, J. D. (2010) *Proc. Natl. Acad. Sci. U.S.A. 107*, 15391−15396]. Here, the 2.17 Å X-ray crystal structure of the archetypal enzyme from the family, CmlA, is reported. CmlA catalyzes β-hydroxylation of L-*p*-aminophenylalanine during chloramphenicol biosynthesis. The fold of the N-terminal domain of CmlA is unlike any previously reported, but the C-terminal domain has the αββα fold of the metallo-β-lactamase (MBL) superfamily. The diiron cluster bound in the C-terminal domain is coordinated by an acetate, three His residues, two Asp residues, one Glu residue, and a bridging oxo moiety. One of the Asp ligands forms an unusual monodentate bridge. No other oxygen-activating diiron enzyme utilizes this ligation or the MBL protein fold. The N-terminal domain facilitates dimerization, but using computational docking and a sequence-based structural comparison to homologues, we hypothesize that it likely serves additional roles in NRPS recognition and the regulation of O_2 activation.

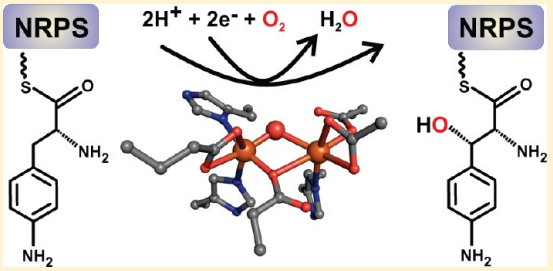

Biosynthesis of many complex secondary metabolites by bacteria and fungi is effected by nonribosomal peptide synthetases (NRPSs). These large, modular enzymes act as "assembly lines" in which each module plays a role in extending or modifying the growing natural product.[1] Generally, a parent amino acid or adduct is covalently tethered to the 4′-phosphopantetheine (PPant) moiety of a modified serine residue on a peptidyl-carrier protein (PCP) domain of the first module of the NRPS by the action of a preceding adenylation (A) domain. The resulting *S*-acyl amino acid intermediates are either chemically modified by following NRPS domains or transferred to the *S*-acyl-linked amino acid adduct on the PCP domain of the next module by the action of a condensation (C) (or similar) domain, forming a new peptide bond. When the synthesis is complete, the natural product is released by the action of a thioesterase (TE) or a reductase (R) domain.

In some cases, the chemical modifications of the developing natural product are catalyzed by "tailoring" enzymes that are not modules of the NRPS but are rather encoded elsewhere, often in the same genetic operon.[1] A common modification for tethered amino acids is β-hydroxylation, which is crucial for the function of many natural products, including the vancomycin and coumarin antibiotic families as well as the antitumor compounds of the bleomycin family.[2,3] The newly introduced hydroxyl function can serve as a site for glycosylation or act as a nucleophile during release of the natural product from the NRPS to form large macrocyclic molecules. A study of the structural and regulatory mechanisms that control the specificity and spatiotemporal activity of these accessory enzymes is necessary to understand the biosynthetic origins of complex natural products. Learning how to harness these capabilities may allow the production of new antibiotics and pharmaceuticals.[4,5]

Sequencing of the chloramphenicol biosynthetic operon[6] led to the discovery of a tailoring enzyme (CmlA) that catalyzes β-hydroxylation of the precursor molecule L-*p*-aminophenylalanine (L-PAPA) to form L-*p*-aminophenylserine.[3] This is a key step in chloramphenicol synthesis as illustrated in Figure 1.[7]

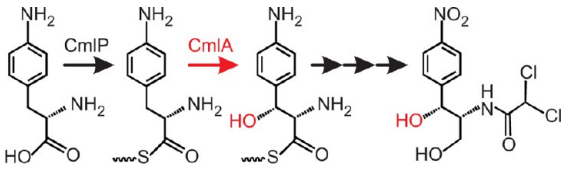

Figure 1. Steps in the biosynthesis of chloramphenicol. The β-hydroxyl colored red is derived from O_2.

The amino acid sequence of CmlA suggests that it has two domains. The N-terminal domain has no known homologues, but the C-terminal domain contains the signature sequence of the αββα-type metallo-β-lactamase (MBL) superfamily.[3,8] The vast majority of MBLs catalyze hydrolysis reactions utilizing a dizinc cluster coordinated by the signature His-X-His-X-Asp-His scaffold, although MBLs with both mono- and dimetal

Received: June 29, 2013
Revised: August 13, 2013
Published: August 27, 2013

   dx.doi.org/10.1021/bi400845b | *Biochemistry* 2013, 52, 6662−6671

clusters containing other metals are known.[9] In contrast, spectroscopic characterization of CmlA showed that it contains a diiron cluster.[3,10]

Prior to the characterization of CmlA, no MBL-like enzymes catalyzing O_2 activation and hydroxylation reactions were known to exist, although a branch of the MBL family that utilizes a diiron cluster to reduce O_2 or NO in obligate anaerobes has been described.[9,11] Typically, β-hydroxylation reactions in NRPS pathways are catalyzed by α-ketoglutarate-dependent oxygenases or cytochrome P450s.[2] CmlA represents a third class, and it is the only known diiron enzyme to catalyze β-hydroxylation of an amino acid-like substrate. Oxygen activation and hydroxylation reactions involving diiron clusters are generally conducted by members of the bacterial multicomponent monooxygenase (BMM) family,[12] which includes enzymes such as the soluble methane monooxygenase (sMMO).[13] In contrast to CmlA, BMMs coordinate the diiron cluster in a four-helix bundle. The typical cluster coordination consists of four carboxylate (Asp/Glu) and two histidine ligands.[14] Numerous kinetic, spectroscopic, and structural studies have shown that both the diiron cluster and the protein scaffold play important roles in orchestrating and regulating the oxygenation chemistry.[13,15,16]

Genome database searching based on the CmlA gene sequence has now shown that there are many enzymes serving similar roles in natural product biosynthesis that are homologous to both the N- and C-terminal regions of CmlA.[3] To date, no enzyme from this group of homologous enzymes has been structurally characterized, and no role for the N-terminal domain has been forthcoming.

Here, we present the crystal structure of CmlA at 2.17 Å resolution. The structure confirms the predicted MBL C-terminal fold and reveals the structure of the N-terminal domain. The detailed structure of the dinuclear iron cluster differs from those of previously characterized oxidoreductases from the MBL family, as well as those from the O_2-activating BMM family. The overall organization of the enzyme suggests different roles for the N- and C-terminal regions as well as the basis for regulation of O_2 activation through interaction with the NRPS from the chloramphenicol biosynthetic pathway, CmlP.

EXPERIMENTAL PROCEDURES

Crystallization of CmlA. CmlA and CmlP were expressed, purified, and quantified as previously described.[3] Crystals of resting CmlA were acquired by the hanging drop vapor diffusion method at 277 K by addition of 3 μL of a 15 mg/mL solution of CmlA in 50 mM HEPES (pH 7.5) to an equal volume of mother liquor containing 100 mM HEPES (pH 7.5), 10−15% polyethylene glycol (formula weight of 20000), 100 mM potassium acetate, and 10% glycerol. Square-bipyramidal CmlA crystals typically grew to 0.2−0.6 mm over the course of several days. Selenomethionine-labeled CmlA was generated by feedback inhibition during expression.[17] Crystals were soaked in mother liquor supplemented with 25% glycerol prior to looping and flash-freezing in liquid nitrogen. For the amino acid cocrystallization, crystallization and freezing conditions were identical to the non-cocrystallized samples except the mother liquor and cryoprotectant contained L-phenylalanine, L-tyrosine, or L-PAPA at final concentrations of 10−20 mM.

Data Collection and Modeling. Data were collected at the Structural Biology Center at the Advanced Photon Source (Argonne National Laboratories, Argonne, IL) on beamline 19-ID at 100 K. Diffraction data were indexed, integrated, and scaled using the HKL2000 software package[18] and phased using single-wavelength anomalous dispersion of the SeMet-labeled enzyme with Phenix.[19] The initial model was prepared with Phenix followed by manual rebuilding. The preliminary model was then used in direct Fourier phasing of a higher-resolution native data set using Refmac5[20] from the CCP4 suite.[21] The final model was prepared using iterative cycles of modeling using Coot[22] and refinement with Refmac5. Iron−ligand bond distances were not restrained during any of the refinement cycles. Model geometries were evaluated using SFCHECK and PROCHECK.[21] X-ray data processing and refinement statistics are listed in Table 1. All structure figures were produced using PyMOL Molecular Graphics System, version 1.5 (Schrödinger, LLC).

Docking of the CmlP PCP Domain and PPant Amino Acid Substrate. Homology modeling of the CmlP PCP domain was performed using Swiss-Model[23] and docked to CmlA using the HADDOCK online server.[24] To guide the docking of the PCP domain, we defined several residues to be part of the interface based on studies of our CmlA model and prior sequence information. For CmlA, we input W438, D496, and H501. These surface residues were chosen on the basis of their proximity to the active site channel. For the CmlP T domain homology model, we input only the serine identified as the putative PPant attachment from sequence comparisons to other structurally characterized PCP domains, with the rationale that this residue must be poised above the channel upon binding of the NRPS to CmlA.

Docking of L-PAPA-PPant to CmlA was performed using the Sybyl-X 2.0 Surflex-Dock Suite (Sybyl-X 2.0 Tripos International, St. Louis, MO). The final CmlA model was prepared by deleting all water molecules and nonprotein ligands, except the Fe atoms, followed by addition of hydrogen to residues. The structure was then minimized using the Amber7 FF99 package in the docking suite, but Fe atoms and ligand positions were unaltered. The substrate was modeled manually in Sybyl-X, and atomic partial charges for both the protein and substrate were automatically calculated and assigned, with the exception of Fe atoms that were manually assigned as +3 and +2 for Fe1 and Fe2, respectively. The parameters for defining the active site were as follows: threshold of 0.65, bloat of 0, and an active site that was automatically identified by the program. The protein was not allowed to flex during docking.

Cloning and Mutagenesis. The expression construct for the E430A mutant of CmlA was produced using an Agilent Quickchange II site-directed mutagenesis kit. The following primer pair was used to introduce the mutation into a pet28a expression plasmid for wild-type (WT) CmlA: CGTCTTCA-TCGGCATGGAGCTCATCGGCGCGG (forward) and CC-GCGCCGATGAGCTCCATGCCGATGAAGACG (reverse). The mutated plasmid was transformed into chemically competent XL1-Blue *Escherichia coli* and plated onto medium containing 50 μg/mL kanamycin. Individual colonies were screened via colony polymerase chain reaction and sequenced to confirm the presence of the mutation. The E430A enzyme was expressed and purified as described above. Mass spectrometry of CmlA was conducted with a QSTAR XL Quadrupole TOF MS instrument from AB Sciex at the University of Minnesota Center for Mass Spectrometry and Proteomics and used to confirm the presence of the desired mutation in the purified enzyme. The deconvoluted mass spectrum showed major peaks at 62204 and 62146 Da for the

dx.doi.org/10.1021/bi400845b | *Biochemistry* 2013, 52, 6662−6671

Table 1. Data Collection and Refinement Statistics[a]

	native	Se-Met
Data Collection		
space group	$P4_32_12$	$P4_32_12$
cell dimensions		
a, *b*, *c* (Å)	153.2, 153.2, 93.4	153.3, 153.3, 92.7
α, *β*, *γ* (deg)	90, 90, 90	90, 90, 90
wavelength (Å)	0.97857	0.97926
resolution (Å)[b]	38.7−2.17 (2.21−2.17)	20.9−2.60 (2.64−2.60)
no. of unique reflections	56972	35553
R_{merge} (%)[b,c]	6.3 (43.5)	10.8 (45.0)
$I/\sigma I$[b]	28 (3.1)	27 (4.5)
completeness (%)[b]	96.4 (81.6)	99.9 (100)
redundancy[b]	7.3 (7.1)	7.2 (7.4)
overall figure of merit		0.405
Cruickshank's diffraction precision index (DPI)	0.154	
Refinement		
resolution (Å)	38.7−2.17	
no. of reflections	54097	
R_{work}/R_{free} (%)[d]	20.3/23.0	
average *B* factor (Å^2)	35.1	
root mean square deviation		
bond lengths (Å)	0.0151	
bond angles (deg)	1.78	
Ramachandran analysis (%)		
favored regions	95.6	
allowed regions	4.0	
disallowed regions	0.4	

[a]All data collected on synchrotron beamline APS SBC-CAT 19ID-D. [b]Data for the highest-resolution shell given in parentheses. [c]$R_{sym} = \sum_{hkl}\sum_i|I_{hkl,i} - \langle I\rangle_{hkl}|/\sum_{hkl}\sum_i|I_{hkl,i}|$, where I_{hkl} is the intensity of a reflection and $\langle I\rangle_{hkl}$ is the average of all observations of the reflection. [d]R_{free} is the *R* factor calculated from 5% of the data excluded from refinement.

WT and E430A mutant, respectively, the difference corresponding to the expected loss of a carboxylate and CH_2 group in the mutant.

Stopped-Flow Kinetics. All stopped-flow experiments were performed with an Applied Photophysics model SX.18MV stopped-flow device at 4 °C. Stopped-flow experiments and CmlP amino acid loading were performed as previously described,[3] with the exception that reduced CmlA was premixed with L-PAPA-loaded $CmlP_{AT}$ in an anaerobic chamber and rapidly mixed with O_2-saturated buffer on the instrument. Excess CmlA reducing reagents and CmlP loading reagents were removed prior to the experiment using a PD10 desalting column.

RESULTS AND DISCUSSION

Overall Structure of CmlA. The structure of CmlA was determined by single-wavelength anomalous dispersion of the selenomethionine-enriched enzyme. The enzyme crystallized in space group $P4_32_12$ with a single monomer in the asymmetric unit. The CmlA model was refined to 2.17 Å resolution with an R_{work} of 0.203 and an R_{free} of 0.230 with 99.6% of the residues in the allowed regions of the Ramachandran plot (Table 1). Overall, 522 residues and 151 solvent molecules were modeled into the electron density map. The CmlA monomer (~62 kDa) is globular with several protrusions that extend from the N-terminal domain (Figure 2 and Figure S1 of the Supporting Information). This domain (residues 1−236, green in Figure 2A) has a mixed *αβ* topology, while the C-terminal domain (residues 249−532, gray with secondary structure indicated in Figure 2A) has the *αββα* topology of the MBL superfamily.[8] The metal cluster and the active site of the enzyme are located in the C-terminal domain, thereby identifying it as the catalytic domain. A stretch of disordered residues separates the domains (residues 237−248, dashed lines in Figure 2). Residues from both domains form the boundaries of a 30 Å long groove that runs along the surface and above the active site channel. These include a kinked *α*-helical region (termed helix N1) composed of residues 26−67 in the N-terminal domain (magenta in Figure 2A) and residues 429−460 (cyan in Figure 2A) and 493−505 from the catalytic domain. A channel located near one end of the groove extends 10 Å from the surface to the active site diiron cluster (Figure 2A, right side). The cluster appears to be easily accessible. This is radically different from that observed in the BMMs, where either the active site is buried deep within the enzyme[25,26] or solvent access is severely restricted.[14,27]

The N-terminal domain is a mixture of *α*-helices and three sets of antiparallel *β*-strands. Structural alignments of this domain made using the Dali Server[28] found no significant matches, with the highest-scoring hit having a calculated root-mean-square deviation (rmsd) of 6.6 Å for the C*α* atoms. This domain is elongated, measuring roughly 70 Å at its longest and 34 Å at its widest. It packs against the catalytic domain through multiple *α*-helices and antiparallel *β*-strands that run parallel to the long axis. A 50 Å long, bent amphipathic helix termed helix N2 (Figure 2) formed by residues 73−107 spans nearly half the length of the domain and perpendicularly packs against helix N1 (residues 27−47). Helix N1 forms an L-shaped arm ("arm 1" in Figure 2A,B) that projects over the catalytic domain forming one side of the groove that runs between the domains.

The overall structure of the catalytic domain is similar to that of other MBLs, having a core of two antiparallel *β*-sheets arranged in a *β*-sandwich flanked by several *α*-helices. On the side that is packed against the N-terminal domain of CmlA, the *α*-helices are notably truncated relative to other members of the MBL superfamily, where these *α*-helices are typically solvent-exposed. On a Dali structural search, the catalytic domain of CmlA is structurally most similar to the MBL L-ascorbate-6-phosphate lactonase UlaG[29] (15% sequence identity, with an rmsd of 2.9 Å for the C*α* atoms). An elongated arm ("arm 2" in Figure 2A,B) is formed by residues 429−460 and extends upward from the *αββα* core (cyan in Figure 2A). Similar extensions have been observed in other members of the MBL superfamily and are relevant to binding[8] and recognition[30] of the substrate in these enzymes. However, the arm in CmlA is longer and has a distinctive orientation. The main portion of

dx.doi.org/10.1021/bi400845b | Biochemistry 2013, 52, 6662−6671

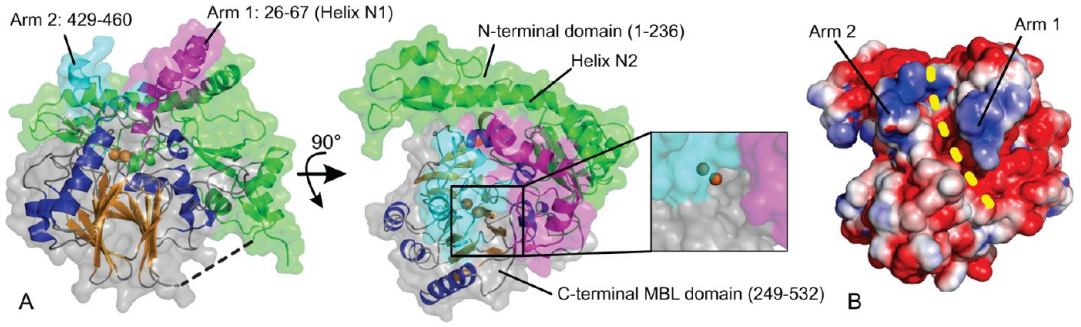

Figure 2. Overall structure of CmlA showing important structural features and electrostatic properties. (A) The N-terminal domain is colored green and the MBL-like catalytic domain gray, with α-helices colored blue and β-sheets colored orange. Iron atoms are displayed as orange spheres. A stretch of disordered residues separates the domains, indicated by the dashed line. Arms extending from CmlA and bordering the surface groove are colored magenta and cyan, and the residue range is shown. The channel to the active site is positioned (see the close-up at the right) at the base of a groove on the surface of CmlA, which runs between arms 1 and 2. (B) Surface electrostatics map of CmlA. The tips of arms 1 and 2 have notable basic character. The surface groove of CmlA lies between these arms and is denoted by the yellow dashed line. The map was generated using APBS[48] and contoured at 2 kT/e.

arm 2 forms one side of the surface groove and active site pocket and, on the opposite face, interacts with another CmlA monomer in the crystal.

Analysis of the crystal packing identified a buried interface of roughly 2700 Å^2 between two CmlA monomers in the unit cell, suggesting the enzyme may function as a dimer in solution. To investigate this possibility, we performed native polyacrylamide gel electrophoresis, which confirmed the dimeric quaternary structure observed in the crystal (Figure S2 of the Supporting Information). A projecting "dimerization arm" (residues 108–146) from the N-terminal domain of CmlA mediates the interaction between the monomers (Figure 3) by packing against the dimerization arm and arm 2 from the symmetry-related protomer. This arrangement places one dimerization arm within 17 Å of the active site of the other protomer.

Structure of the Diiron Cluster. The active site of CmlA is situated above the β-sheets of the $\alpha\beta\beta\alpha$ core of the catalytic domain. Structural alignments of this domain show that the active sites of other members of the MBL superfamily are found in similar spatial positions relative to the rest of the fold. The iron atoms are ligated in part by four ligands derived from a loop containing the conserved metal binding motif, which extends upward between the fourth β-strand and second α-helix of the catalytic domain (Figure 4A and Figure S1 of the Supporting Information). The only apparent access to the active site is from the channel above, although some solvent-occupied caverns can be seen extending from the substrate binding pocket.

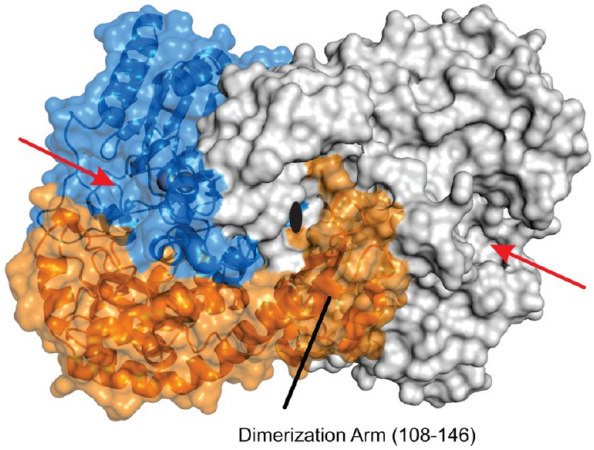

Figure 3. CmlA is a dimer, and the interaction between protomers is mediated by an extension from the N-terminal domain. Shown is a surface view of the CmlA dimer with the dimerization arm and the corresponding residue range indicated. One protomer surface is transparent, with secondary structure shown as a cartoon. In this protomer, the N-terminal domain is colored orange and the catalytic domain blue. The other protomer is colored white. Red arrows indicate the locations of the active site channels. The black oval indicates the location of the 2-fold crystallographic symmetry axis that runs through the dimer.

The two iron atoms in the enzyme active site are in distorted octahedral environments with six ligands each (Figure 4A and Figure S3 of the Supporting Information). Herein, iron atoms are termed Fe1 and Fe2 for Fe600 and Fe601 in the model, respectively. Iron atom occupancies refined to 1.0 for Fe1 and 0.75 for Fe2 (see the Supporting Information). The iron–iron distance was determined to be 3.39 Å, in close agreement with EXAFS studies.[10] The strong density for a bridging atom is also apparent in the difference map following refinement of the cluster (Figure 4B), and on the basis of previous spectroscopic studies of the diferric state of CmlA,[3,10] we have modeled this density with an oxo atom (O602). The iron–oxo bond distances refined to 1.77 and 2.15 Å for Fe1 and Fe2, respectively. EXAFS studies[10] suggested the average iron–oxo distance is ~1.8 Å, raising the possibility that Fe2 may have been reduced to the ferrous state during data collection, forming a mixed-valent (MV) Fe(III)Fe(II) cluster. Consistent with this, the overall average ligand distances refined to 2.0 Å for Fe1 and 2.3 Å for Fe2. We investigated the possibility of reduction during data collection by several standard approaches (Supporting Information). However, none of these methods provided definitive evidence of a mixed-valence (MV) cluster.

The cluster in CmlA is coordinated by one fewer endogenous amino acid carboxylate and one more histidine ligand compared to what is found for most other diiron hydroxylases. All nitrogen ligands derive from the conserved MBL metal-binding scaffold. The N-terminal domain contributes no cluster ligands. Fe2 is coordinated by D309, H310, a monatomic bridging D403, an acetate molecule (ACT603) derived from the crystallization buffer, and the bridging O atom. Fe1 is coordinated by a chelating E377, bridging D403, H305, H307, and the bridging O atom. It is likely that in solution the coordinating acetate is replaced by solvent because

dx.doi.org/10.1021/bi400845b | *Biochemistry* 2013, 52, 6662–6671

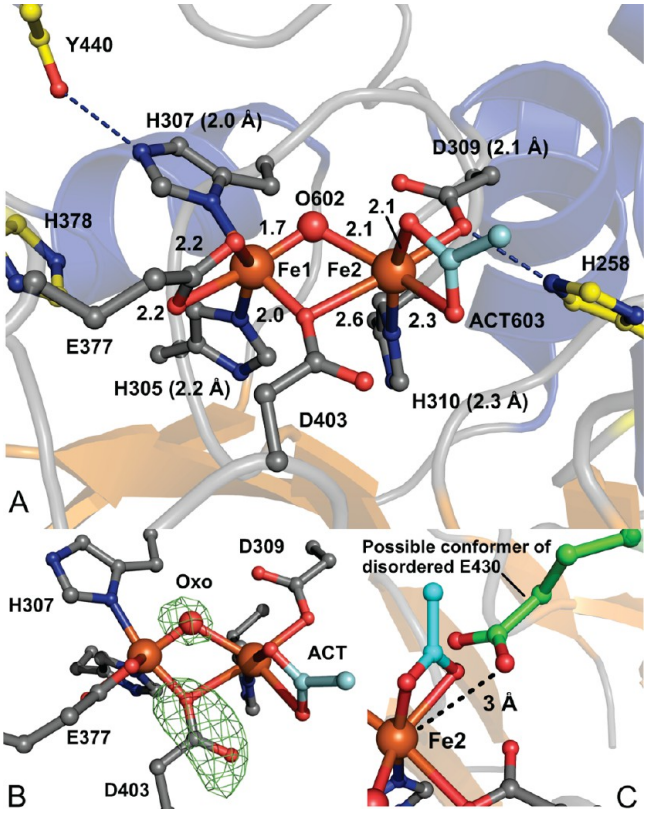

Figure 4. Structure of the CmlA active site and nearby residues. (A) Cluster geometry and bond distances in angstroms, with iron ligands colored gray, second-sphere conserved residues colored yellow, and the bridging oxo atom shown as a red sphere. Blue dashes indicate hydrogen bonds. The exogenous acetate ligand (Act) is colored cyan. When not directly indicated, distances are given in parentheses. (B) Positive $F_o - F_c$ difference electron density (green) following removal of the oxo bridge atom and trimming of D403 back to Ala, followed by five cycles of refinement. $F_o - F_c$ difference electron density contoured at 4σ for the oxo group and 7σ for D403. The map was calculated using a resolution range of 38.7−2.17 Å. (C) One possible rotameric conformation of the disordered E430 side chain (green) places the carboxylate within 3 Å of Fe2, overlapping partially with the acetate (cyan) binding site.

no acetate is added to the purification buffer. Exposure of CmlA to 100 mM potassium acetate in a buffered solution results in no detectable changes in the chromophore.

Monodentate Diiron Cluster Bridging Structure. The monodentate $\mu-\eta^2$ binding mode of D403 in CmlA was unexpected, because in most oxygen activating diiron enzymes and model complexes the carboxylate forms a μ-1,3 bridge. The monodentate bridging mode has been observed in purple acid phosphatase, the reduced form of the D84E mutant of *E. coli* ribonucleotide reductase R2 subunit, and the reduced sMMO hydroxylase component.[31−35] However, in the latter two cases, the bridging mode is μ-(η^1,η^2) where the second oxygen of the carboxylate coordinates to one of the irons. Also, in both cases, a traditional μ-1,3 bridging carboxylate is also present. It is unlikely that D403 in CmlA can assume a μ-1,3 orientation without significant rearrangements of the backbone because of several constraints: (i) D403 is sterically restrained and essentially limited to rotation around the Cβ−Cγ bond, (ii) D403 needs to rotate toward Fe1 to bring the second oxygen close enough to coordinate Fe2; this would introduce severe strain on the sp^3 hybridization of the D403 Cα atom and would result in steric clashes with E377 and an overly short iron−oxygen bond to Fe1. Finally, (iii) if the backbone rearranges, it would be required to undergo a nearly 90° rotation to bring the carboxylate into an allowed conformation close enough to coordinate both metals. Indeed, rubredoxin:oxygen oxidoreductase has a bidentate Asp bridge, and the backbone runs perpendicular to the iron−iron axis; in CmlA and purple acid phosphatase, the backbone runs more parallel. Thus, the bridge in CmlA is essentially "locked" into a single orientation during the catalytic cycle in the absence of significant structural rearrangement.

Structure of the Substrate Binding Pocket. The substrate binding pocket is elongated, roughly 8 Å × 13 Å (Figure 5). The pocket is bordered on one side by L458 and I439, on the opposite side by M493 and V492, and on top by the partially disordered surface-exposed W438, which sits at the base of the surface groove between domains. Q308 is positioned 8 Å from the cluster at the opposite end of the active site pocket, as measured from the Q308 carboxamide to the O602 in the cluster ("conformation 1"). A second conformation ("conformation 2") of Q308 observed in the electron density map positions the side chain farther from the

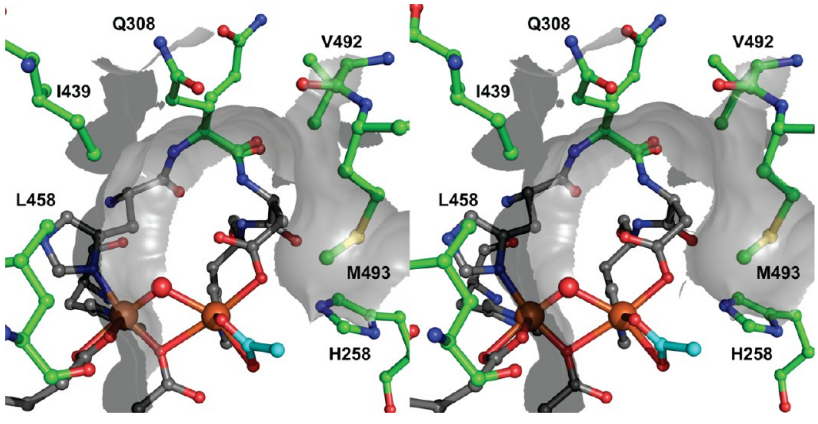

Figure 5. Stereoview diagram of the CmlA active site pocket as viewed from the channel. Residues that form the pocket are colored green and labeled. The cluster is represented as in Figure 4. Gray surface contours illustrate the shape of the pocket and define a likely binding orientation for the aromatic substrate. W438 is positioned above the pocket and has been omitted for the sake of clarity.

dx.doi.org/10.1021/bi400845b | *Biochemistry* 2013, 52, 6662−6671

cluster, expanding the long dimension of the binding pocket (Figure S4 of the Supporting Information). Y440 is at the back of the pocket and appears to engage in a hydrogen bond with the ε-nitrogen of Fe1 ligand H307 (Figure 4A).

In all models, additional areas of residual positive $F_o - F_c$ density were observed in the part of the pocket above the cluster. We attempted to model this density with solvent molecules, but this resulted in significant residual positive density after refinement. Cocrystals of CmlA with 10−20 mM amino acids L-tyrosine, L-phenylalanine, and L-PAPA resulted in isomorphous crystals, but insufficient density to model any amino acid substrates in the binding pocket. This density appeared to be nearly identical to that observed in crystals that were not cocrystallized with amino acids (Figure S5 of the Supporting Information) and does not correspond well with components of the crystal mother liquor; thus, its source remains unknown. The absence of significant electron density for any amino acids in these cocrystallized samples demonstrates that free amino acids have little affinity for binding in the CmlA active site. This was also observed in a cytochrome P450 tailoring system in which no amino acid binding was detected even with a 500-fold excess over protein. In contrast, the NPRS-tethered substrate had a binding affinity in the low micromolar range.[36] The possible binding mode of the NRPS-bound substrate in CmlA is discussed and modeled in context below.

The monooxygenase chemistry catalyzed by CmlA requires delivery of two protons and two electrons to the reactive center during turnover, leading to release of a water molecule. We searched for possible endogenous proton donors in CmlA. One candidate is H258, which is positioned only 3 Å from Fe2 in the same plane as the cluster (Figure 4A). Ramachandran analysis shows H258 to be in a strained orientation, likely because the residue engages in a hydrogen bond with D309. On the opposite side, another His residue, H378, is positioned 5 Å from Fe1 but points away from the cluster. Alternatively, the surface-exposed E430 could act as a proton shuttle from bulk solvent.

Conserved Structural Features of CmlA and Homologues. The structure of CmlA permits the sequence-based structural comparison of family members. To identify residues that may be functionally relevant, we generated an alignment of CmlA with 13 homologues from diverse species, which have 32−41% sequence identity (Table S1 of the Supporting Information). In the N-terminal domain, the conserved residues appear to primarily serve structural roles by engaging in interactions with nearby residues or facilitating turns on the protruding arms (Figure 6, G110). A cluster of conserved residues also appears to stabilize the dimerization arm in the N-terminal domain (Figure S6 of the Supporting Information). S44 and H52 engage in a hydrogen bonding interaction that maintains a kink in helix N1. The similar length and high level of sequence identity of the homologues (Table S1 of the Supporting Information), along with the nature of the noted conservations, indicate that the overall shape of the N-terminal domain is conserved. However, the intervening regions are highly variable in their chemical character, including in helix N2 (residues 73−107) and in the tips of arms 1 and 2 (Figure S6 of the Supporting Information). In the active site of the catalytic domain, all of the iron ligands, W441, Y443, and potential proton donors H258, H378, and E430, are conserved in all homologues. None of the residues that line the binding pocket (I439, L458, V492, M493, and Q308) are conserved.

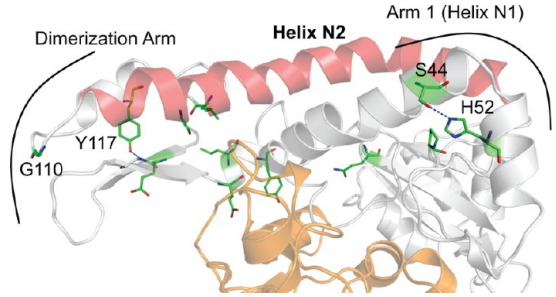

Figure 6. Conserved residues of the N-terminal domain identified from sequence alignments with CmlA homologues and mapped onto the crystal structure. Conserved residues are colored green, with the catalytic domain colored orange and the N-terminal domain colored white. Residues primarily serve structural roles by interacting with nearby residues through hydrogen bonds and hydrophobic packing or facilitating turns on the arms (G110). Two hydrogen-bonded pairs are denoted by blue dashed lines: S44 and H52 and Y117 and the amide of a nearby residue. Helix N2 in the N-terminal domain is colored red.

Putative electron delivery routes have been identified in other diiron enzymes,[37] and we attempted to find such a route in CmlA and to identify a possible ferredoxin (Fd) or flavo-iron-sulfur reductase interaction site. From the sequence alignments, we noted a partially conserved buried aromatic network starting at the solvent-exposed Y479 that runs to underneath the cluster through the interior of the catalytic domain terminating at Y255, which is hydrogen bonded to the carbonyl group of H258 (Figure 7A). In more distant homologues, some

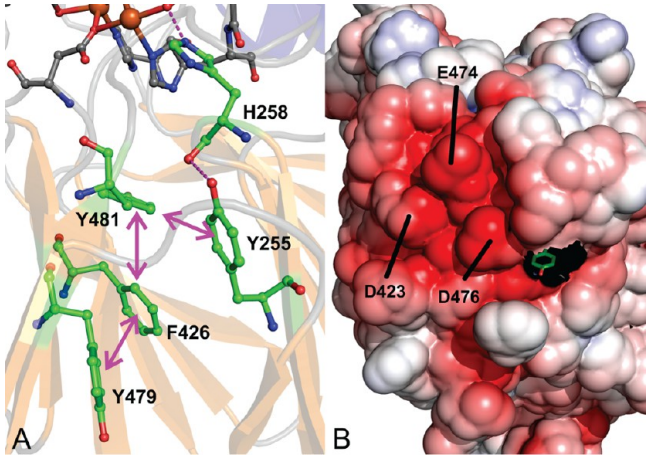

Figure 7. Identification of a possible electron delivery network and reductase binding site in CmlA. (A) Conserved aromatic network that extends from solvent-exposed Y479 to the diiron cluster. (B) Surface electrostatics map of CmlA showing a possible acidic binding site at the base of the catalytic domain. Y479 is drawn as sticks colored by atom (green for carbon). The map was generated using APBS[48] and contoured at 5 kT/e.

positions are substituted with other aromatic residues. CmlA surface electrostatics reveal a strongly acidic patch (residues D423, E474, D476, and E477) at the base of the catalytic domain (Figure 7B) that might form a binding site for an electron transfer partner. Y479 is next to this patch and engages in a hydrogen bond with the carboxylate of E477. The acidic nature of this region would be more compatible with direct electron transfer from a flavo-iron-sulfur reductase[38] than a Fd,[39] which is likely to carry a strong negative charge.

dx.doi.org/10.1021/bi400845b | Biochemistry 2013, 52, 6662−6671

Unfortunately, a specific reductase protein for CmlA has not been identified, and the Cml operon appears not to encode such a protein.[6] Thus, a definitive test of this hypothesis through mutagenesis is not currently possible.

Interaction of CmlA with the NRPS. CmlA hydroxylates only L-PAPA tethered to the carrier PCP domain of CmlP via a thioester bond to a PPant linker, minimally necessitating a specific interaction between the holo-PCP domain and CmlA. To identify the binding site of the PCP domain of CmlP and elucidate possible features conferring NRPS specificity, we docked a homology model of the highly conserved CmlP PCP domain[40,41] to the crystal structure of CmlA (Figure 8 and blue

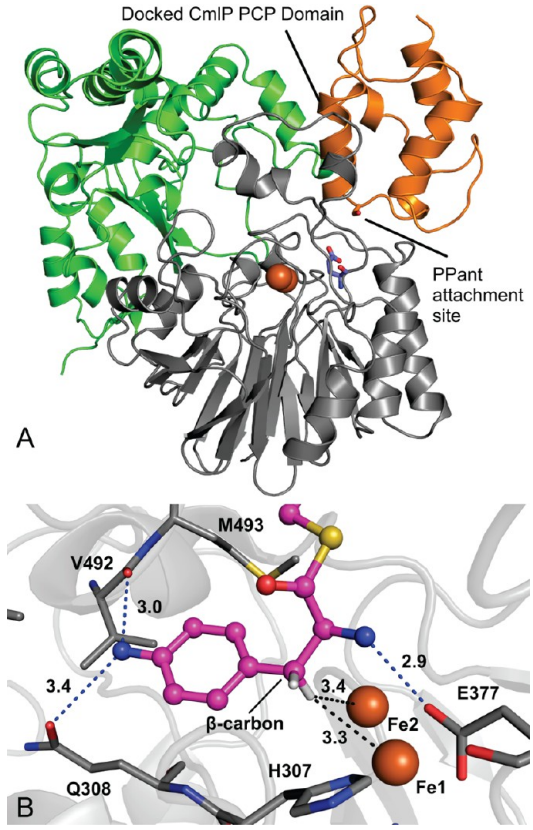

Figure 8. Computationally docked structures. (A) Homology-modeled CmlP PCP domain and CmlA. The PCP domain likely binds above the channel to the active site but interacts minimally with the N-terminal domain. The PCP domain is colored orange with the putative PPant attachment site labeled. The CmlA N-terminal and catalytic domains are colored green and gray, respectively. E430 is positioned on a loop below the putative PCP domain binding site and is colored blue. (B) Model of the PPant-L-PAPA substrate docked in the active site of CmlA. PPant-L-PAPA is colored magenta. Protein residues are colored gray. Hydrogens on the β-carbon are colored white. All distances are in angstroms. Hydrogen bonds are indicated by blue dashes. Docking was performed using Sybyl-X 2.0.

residues in Figure S6 of the Supporting Information). In this model, the carrier protein binds directly above the channel to the active site, as observed in similar systems,[42] and the serine residue where the PPant cofactor attaches is poised above the channel to the active site. The PCP domain interacts primarily with arm 2 that extends from the catalytic domain of CmlA and the residues around the channel to the active site. The binding site is minimally conserved (Figure S6 of the Supporting Information), which is consistent with the high specificity of the hydroxylation reaction.

Sequence-based structural comparisons of CmlA and homologues show that the surface composition of the N-terminal domain is highly variable. Nevertheless, there are 12 conserved residues, and these appear to be required to maintain the overall folded structure of each of the protruding arms on CmlA. This suggests that each arm is functionally relevant, but the small size of the CmlP carrier domain would limit its interaction to a portion of the arms identified in the docked model (Figure S6 of the Supporting Information). Analysis of CmlA surface electrostatics reveals that the tips of the arms, which form the groove between domains, have a net positive charge relative to the rest of the surface (Figure 2C), suggesting that it may be used as a mechanism for electrostatically targeting the correct NRPS. One interpretation is that the NRPS specificity of the *trans*-acting tailoring enzymes from the CmlA family is conferred by interactions with the entire NRPS module and not just the CmlP carrier domain. Resolution of this possibility awaits further study.

NRPS-Loaded Substrate Binding in the Active Site of CmlA. In the $P450_{biol}$-ACP crystal complex, the PPant-tethered substrate is funneled into a long U-shaped cavity that positions the hydroxylation site above the heme for oxidation.[42] We propose that a similar mechanism functions in CmlA, and that substrate positioning is primarily directed by the shape of the pocket and the length restraints of the linker, resulting in the positioning of the β-carbon of L-PAPA above the cluster. The shape of the pocket suggests an orientation in which the substrate-tethered PPant linker bends roughly 45° over the cluster, toward Q308 and between the side chains of M493 and I439 (Figure 5). The length of the linker requires that the substrate be pushed farther down toward Q308, with the aromatic portion extending beyond the cluster. The Q308 side chain may then adopt conformation 2 (Figure S4 of the Supporting Information) farther back in the pocket, accommodating the substrate and stabilizing it in a specific orientation through hydrogen bonding to the *p*-NH_2 group of L-PAPA. In CmlA homologues, Q308 is substituted with other residues capable of H-bonding to substrate. In Tyr-accepting homologues (from *Actinoplanes teichomyceticus*, *Nonomurea* sp., and *Streptomyces toyocaensis*) involved in the synthesis of teicoplanins and other glycopeptides, Q308 is substituted with Ser. In a putative His-accepting homologue from *Streptomyces verticillus* involved in bleomycin synthesis, Q308 is replaced with His (Table S1 of the Supporting Information). The β-carbon of L-PAPA is the site of hydroxylation and must be positioned near the cluster after binding of the substrate. In our docked CmlA-PCP domain model, the distance between the PPant attachment site and the cluster is 13 Å, which matches well with observations from other systems.[42,43] Once binding has occurred, this would position the L-PAPA amide somewhere above the cluster and β-carbon slightly beyond it, near the site occupied by the oxo bridge in the resting state structure.

To test this possibility, we docked a model of the PPant-L-PAPA substrate to our structure of CmlA (Figure 8B). We separately docked the substrate to CmlA with Q308 in each conformation (Figure S4 of the Supporting Information), but only conformation 2 shown in Figure 8B gave a result consistent with the observed chemistry. In this model, the aromatic group of L-PAPA is positioned in the pocket identified in Figure 5, and the *p*-NH_2 group interacts with nearby

dx.doi.org/10.1021/bi400845b | *Biochemistry* 2013, 52, 6662−6671

carbonyl groups from V492 and the side chain of Q308. The β-carbon is positioned above the cluster, with the correct prochiral hydrogen placed within 3.4 Å of both Fe atoms. These results support our proposed binding orientation and are consistent with a role for Q308 in orienting the substrate in the pocket.

Regulation of Oxygen Activation. Intermediates formed during O_2 activation are potentially dangerous oxidants to living systems.[44,45] BMMs have evolved sophisticated regulatory mechanisms for generating these oxidizing species only in the presence of substrate and/or regulatory protein binding partners to mitigate undesired side reactions.[13,25,27,46] The triggering of O_2 activation by CmlA only upon binding to substrate-loaded CmlP is a salient example, and it implies a regulatory role for the NRPS.[3] The mechanism of regulation of O_2 activation in the BMM family often involves structural changes. For example, the binding of regulatory protein MMOB to the hydroxylase component of sMMO causes structural changes near the diiron cluster,[27,47] and similar perturbations may also occur in CmlA. Comparison of the predicted and observed cluster ligand structures of CmlA suggests a possible regulatory mechanism.

In our earlier study, the cluster ligands reported here were correctly predicted on the basis of sequence comparisons to other members of the MBL superfamily and alignments to CmlA homologues.[3] However, E430 was also identified as a likely fourth carboxylate ligand to the diiron cluster. Analysis of the electron density maps shows that this residue is positioned nearby on a loop (residues 430−437) that runs along the base of the groove between the domains above the acetate binding site of Fe2. It does not coordinate the cluster, and the side chain of E430 appears to be disordered. One possible rotameric conformation of E430 places the carboxylate group within ∼3 Å of Fe2 (green in Figure 4C), an orientation that partially overlaps with the acetate ligand [and the solvent(s) that presumably replaces the acetate when the enzyme is in solution]. The residue is sufficiently distant that it cannot coordinate to the cluster without a concomitant shift in the backbone. Coordination of E430 to Fe2 would build the carboxylate rich diiron cluster that differentiates O_2 carrier proteins from O_2 activating enzymes.[3,10] Consequently, a conformational change that allows E430 to coordinate might serve as the switch to promote O_2 activation. E430 is located on a loop directly below the tentative binding site of the CmlP PCP domain identified in the docked structure (blue residue in Figure 8A), so that the docking of CmlP may shift E430 close enough to coordinate to Fe2. Conservation of the nearby G433 residue could indicate it is required to maintain the backbone flexibility required for this change.

An initial examination of the hypothesized role of E430 was made using the E430A variant. A single turnover of fully reduced E430A in complex with L-PAPA-loaded $CmlP_{AT}$ resulted in a 25-fold decrease in the maximal rate constant for reaction with O_2 as shown in Figure 9. In contrast, the autoxidation rate in the absence of L-PAPA-loaded CmlP was unchanged from that observed for WT CmlA. The total iron loading in the active site of the E430A variant was comparable to that of WT CmlA but exhibited a blue-shifted optical absorption spectrum (Figure S7 of the Supporting Information). This demonstrates that E430 interacts strongly with the diiron cluster despite its position being remote from Fe2. As expected, the optical spectra of diferrous CmlA and E430, with or without L-PAPA-loaded $CmlP_{AT}$ bound, were bleached and

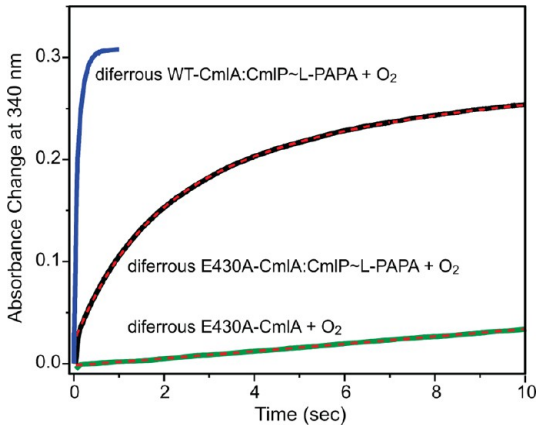

Figure 9. Stopped-flow reaction between 100 μM chemically reduced WT or E430A CmlA in complex with a 2.5-fold excess of L-PAPA-loaded $CmlP_{AT}$ rapidly mixed with O_2-saturated buffer at 4 °C and pH 7.5. The reaction of WT CmlA (blue) is complete within 1 s ($1/\tau_1$ = 17 s^{-1}, and $1/\tau_2$ = 5.2 s^{-1}). The E430A reaction (black) can be fit by a sum of three exponentials (red dashed) with the following: $1/\tau_1$ = 0.68 ± 0.09 s^{-1}, $1/\tau_2$ = 0.18 ± 0.04 s^{-1}, and $1/\tau_3$ = 0.020 ± 0.006 s^{-1}. The basis for the multiple-exponential time course is unknown. Autoxidation of the cluster upon exposure of reduced E430A to O_2 in the absence of CmlP (green) can be fit (red dashed) to a single exponential with a $1/\tau_1$ of 0.014 ± 0.007 s^{-1}, the same as that observed for WT CmlA autoxidation. The reaction of WT CmlA (blue) is from ref 3.

featureless in the visible range.[3] These results support the hypothesis that E430 has a role in establishing a diiron cluster structure that is capable of rapidly activating O_2. However, the fact that E430A still accelerates the rate of O_2 reaction over autoxidation (Figure 9) suggests that the complex with the loaded NRPS has additional structural and/or electronic effects on this reaction. Initial attempts to crystallize E430A were successful, but the resulting crystal forms did not diffract to high resolution.

■ CONCLUSION

Tailoring of natural products during biosynthesis in NRPS-based systems is highly specific. The X-ray crystal structure of the archetypal diiron cluster-containing β-hydroxylase from an NRPS system described here provides insight into the basis for this specificity. It is likely to involve interactions directly with the substrate, L-PAPA, in the CmlA active site and also with the NRPS to which L-PAPA is covalently attached. The two structural domains identified in CmlA may serve different roles in establishing specificity. The structure demonstrates directly that the C-terminal domain houses the active site in which the diiron cluster responsible for oxygen activation is bound. The full role of the N-terminal domain with its previously uncharacterized structural motif remains open to speculation. While the structure shows that this domain facilitates dimerization in this family of enzymes, its proximity to the channel into the active site and the structural conservation of CmlA homologues also imply a role in establishing the NRPS complex. Finally, the NRPS may also act as a regulator of O_2 activation, delivering substrate and engendering conformational changes in CmlA that ensure that the oxidative chemistry occurs only in the presence of the tethered amino acid.

dx.doi.org/10.1021/bi400845b | Biochemistry 2013, 52, 6662−6671

■ ASSOCIATED CONTENT

Supporting Information

One table and seven figures. This material is available free of charge via the Internet at http://pubs.acs.org.

Accession Codes

The crystallography statistics, atomic coordinates, and structure factors coordinates have been deposited in the Protein Data Bank as entry 4JO0.

■ AUTHOR INFORMATION

Corresponding Authors

*E-mail: wilmo004@umn.edu. Telephone: (612) 624-2406. Fax: (612) 624-5121.

*E-mail: Lipsc001@umn.edu. Telephone: (612) 625-6454. Fax: (612) 624-5121.

Present Address

†Department of Chemistry and Biochemistry, University of South Carolina, 631 Sumter St., Columbia, SC 29208.

Author Contributions

T.M.M. and C.J.K. contributed equally to this work.

Funding

This work was supported by National Institutes of Health Grants GM40466 (to J.D.L.), GM40466-S1 (to J.D.L.), GM100943 (to J.D.L.), and GM66569 (to C.M.W.) and Graduate Traineeship GM008700 (to C.J.K.).

Notes

The authors declare no competing financial interest.

■ ACKNOWLEDGMENTS

We thank Drs. Lawrence Que, Jr., and Erik Yukl for valuable discussions. Diffraction data were collected at Argonne National Laboratory, Structural Biology Center at the Advanced Photon Source. Argonne National Laboratory is operated by UChicago Argonne, LLC, for the U.S. Department of Energy, Office of Biological and Environmental Research, under Contract DE-AC02-06CH11357. We are grateful for resources from the Supercomputing Institute and the Kahlert Center for Structural Biology at the University of Minnesota.

■ ABBREVIATIONS

NRPS, nonribosomal peptide synthetase; CmlA, β-hydroxylase of the chloramphenicol biosynthetic pathway; CmlP, NRPS of the chloramphenicol biosynthetic pathway; sMMO, soluble form of methane monooxygenase; MMOB, regulatory component B of the sMMO system; L-PAPA, L-*p*-aminophenylalanine; PPant, 4′-phosphopantetheine cofactor; PCP, peptidyl-carrier protein [this CmlP domain contains the serine attachment site for PPant and the amino acid substrates that are subsequently covalently linked to PPant; PCP is alternatively termed the thiolation (T) domain]; $CmlP_{AT}$, truncated version of full-length CmlP lacking the C-terminal reductase domain of the NRPS.

■ REFERENCES

(1) Fischbach, M. A., and Walsh, C. T. (2006) Assembly-line enzymology for polyketide and nonribosomal peptide antibiotics: Logic, machinery, and mechanisms. *Chem. Rev. 106*, 3468−3496.

(2) Chen, H., Thomas, M. G., O'Connor, S. E., Hubbard, B. K., Burkart, M. D., and Walsh, C. T. (2001) Aminoacyl-S-enzyme intermediates in β-hydroxylations and α,β-desaturations of amino acids in heptide antibiotics. *Biochemistry 40*, 11651−11659.

(3) Makris, T. M., Chakrabarti, M., Münck, E., and Lipscomb, J. D. (2010) A family of diiron monooxygenases catalyzing amino acid β-hydroxylation in antibiotic biosynthesis. *Proc. Natl. Acad. Sci. U.S.A. 107*, 15391−15396.

(4) Nguyen, K. T., Ritz, D., Gu, J.-Q., Alexander, D., Chu, M., Miao, V., Brian, P., and Baltz, R. H. (2006) Combinatorial biosynthesis of novel antibiotics related to daptomycin. *Proc. Natl. Acad. Sci. U.S.A. 103*, 17462−17467.

(5) Zhang, C., Griffith, B. R., Fu, Q., Albermann, C., Fu, X., Lee, I.-K., Li, L., and Thorson, J. S. (2006) Exploiting the reversibility of natural product glycosyltransferase-catalyzed reactions. *Science 313*, 1291−1294.

(6) He, J., Magarvey, N., Piraee, M., and Vining, L. C. (2001) The gene cluster for chloramphenicol biosynthesis in *Streptomyces venezuelae* ISP5230 includes novel shikimate pathway homologues and a monomodular non-ribosomal peptide synthetase gene. *Microbiology 147*, 2817−2829.

(7) Doull, J., Ahmed, Z., Stuttard, C., and Vining, L. C. (1985) Isolation and characterization of *Streptomyces venezuelae* mutants blocked in chloramphenicol biosynthesis. *J. Gen. Microbiol. 131*, 97−104.

(8) Bebrone, C. (2007) Metallo-β-lactamases (classification, activity, genetic organization, structure, zinc coordination) and their superfamily. *Biochem. Pharmacol. 74*, 1686−1701.

(9) Frazão, C., Silva, G., Gomes, C. M., Matias, P., Coelho, R., Sieker, L., Macedo, S., Liu, M. Y., Oliveira, S., Teixeira, M., Xavier, A. V., Rodrigues-Pousada, C., Carrondo, M. A., and Le Gall, J. (2000) Structure of a dioxygen reduction enzyme from *Desulfovibrio gigas*. *Nat. Struct. Mol. Biol. 7*, 1041−1045.

(10) Vu, V. V., Makris, T. M., Lipscomb, J. D., and Que, L. (2011) Active-site structure of a β-hydroxylase in antibiotic biosynthesis. *J. Am. Chem. Soc. 133*, 6938−6941.

(11) Silaghi-Dumitrescu, R., Kurtz, D. M., Jr., Ljungdahl, L. G., and Lanzilotta, W. N. (2005) X-ray crystal structures of *Moorella thermoacetica* FprA. Novel diiron site structure and mechanistic insights into a scavenging nitric oxide reductase. *Biochemistry 44*, 6492−6501.

(12) Notomista, E., Lahm, A., Di Donato, A., and Tramontano, A. (2003) Evolution of bacterial and archaeal multicomponent monooxygenases. *J. Mol. Evol. 56*, 435−445.

(13) Wallar, B. J., and Lipscomb, J. D. (1996) Dioxygen activation by enzymes containing binuclear non-heme iron clusters. *Chem. Rev. 96*, 2625−2657.

(14) Rosenzweig, A. C., Frederick, C. A., Lippard, S. J., and Nordlund, P. (1993) Crystal structure of a bacterial non-haem iron hydroxylase that catalyses the biological oxidation of methane. *Nature 366*, 537−543.

(15) Kovaleva, E. G., Neibergall, M. B., Chakrabarty, S., and Lipscomb, J. D. (2007) Finding intermediates in the O_2 activation pathways of non-heme iron oxygenases. *Acc. Chem. Res. 40*, 475−483.

(16) Tinberg, C. E., and Lippard, S. J. (2011) Dioxygen activation in soluble methane monooxygenase. *Acc. Chem. Res. 44*, 280−288.

(17) Van Duyne, G. D., Standaert, R. F., Karplus, P. A., Schreiber, S. L., and Clardy, J. (1993) Atomic structures of the human immunophilin FKBP-12 complexes with FK506 and rapamycin. *J. Mol. Biol. 229*, 105−124.

(18) Otwinowski, Z., and Minor, W. (1997) Processing of X-ray diffraction data collected in oscillation mode. *Methods Enzymol. 276*, 307−326.

(19) Adams, P. D., Afonine, P. V., Bunkóczi, G., Chen, V. B., Davis, I. W., Echols, N., Headd, J. J., Hung, L.-W., Kapral, G. J., Grosse-Kunstleve, R. W., McCoy, A. J., Moriarty, N. W., Oeffner, R., Read, R. J., Richardson, D. C., Richardson, J. S., Terwilliger, T. C., and Zwart, P. H. (2010) PHENIX: A comprehensive Python-based system for macromolecular structure solution. *Acta Crystallogr. D66*, 213−221.

(20) Murshudov, G. N., Vagin, A. A., and Dodson, E. J. (1997) Refinement of macromolecular structures by the maximum-likelihood method. *Acta Crystallogr. D53*, 240−255.

(21) Winn, M. D., Ballard, C. C., Cowtan, K. D., Dodson, E. J., Emsley, P., and Evans, P. R. (2011) Overview of the CCP4 suite and current developments. *Acta Crystallogr. D67*, 235−242.
(22) Emsley, P., and Cowtan, K. (2004) Coot: Model-building tools for molecular graphics. *Acta Crystallogr. D60*, 2126−2132.
(23) Kiefer, F., Arnold, K., Künzli, M., Bordoli, L., and Schwede, T. (2009) The SWISS-MODEL Repository and associated resources. *Nucleic Acids Res. 37*, D387−D392.
(24) de Vries, S. J., van Dijk, M., and Bonvin, A. M. J. J. (2010) The HADDOCK web server for data-driven biomolecular docking. *Nat. Protoc. 5*, 883−897.
(25) Bailey, L. J., McCoy, J. G., Phillips, G. N., Jr., and Fox, B. G. (2008) Structural consequences of effector protein complex formation in a diiron hydroxylase. *Proc. Natl. Acad. Sci. U.S.A. 105*, 19194−19198.
(26) Sazinsky, M. H., Bard, J., Di Donato, A., and Lippard, S. J. (2004) Crystal structure of the toluene/o-xylene monooxygenase hydroxylase from *Pseudomonas stutzeri* OX1. Insight into the substrate specificity, substrate channeling, and active site tuning of multi-component monooxygenases. *J. Biol. Chem. 279*, 30600−30610.
(27) Lee, S. J., McCormick, M. S., Lippard, S. J., and Cho, U.-S. (2013) Control of substrate access to the active site in methane monooxygenase. *Nature 494*, 380−384.
(28) Holm, L., and Rosenström, P. (2010) Dali server: Conservation mapping in 3D. *Nucleic Acids Res. 38*, W545−W549.
(29) Garces, F., Fernández, F. J., Montellà, C., Penya-Soler, E., Prohens, R., Aguilar, J., Baldomà, L., Coll, M., Badia, J., and Vega, M. C. (2010) Molecular architecture of the Mn^{2+}-dependent lactonase UlaG reveals an RNase-like metallo-β-lactamase fold and a novel quaternary structure. *J. Mol. Biol. 398*, 715−729.
(30) de la Sierra-Gallay, I. L., Pellegrini, O., and Condon, C. (2005) Structural basis for substrate binding, cleavage and allostery in the tRNA maturase RNase Z. *Nature 433*, 657−661.
(31) Strater, N., Klabunde, T., Tucker, P., Witzel, H., and Krebs, B. (1995) Crystal structure of a purple acid phosphatase containing a dinuclear Fe(III)-Zn(II) active site. *Science 268*, 1489−1492.
(32) Voegtli, W. C., Khidekel, N., Baldwin, J., Ley, B. A., Bollinger, J. M., Jr., and Rosenzweig, A. C. (2000) Crystal structure of the ribonucleotide reductase R2 mutant that accumulates a μ-1,2-peroxodiiron(III) intermediate during oxygen activation. *J. Am. Chem. Soc. 122*, 3255−3261.
(33) Rosenzweig, A. C., Nordlund, P., Takahara, P. M., Frederick, C. A., and Lippard, S. J. (1995) Geometry of the soluble methane monooxygenase catalytic diiron center in two oxidation states. *Chem. Biol. 2*, 409−418.
(34) Whittington, D. A., and Lippard, S. J. (2001) Crystal structures of the soluble methane monooxygenase hydroxylase from *Methylococcus capsulatus* (Bath) demonstrating geometrical variability at the dinuclear iron active site. *J. Am. Chem. Soc. 123*, 827−838.
(35) Wei, P.-p., Skulan, A. J., Mitić, N., Yang, Y.-S., Saleh, L., Bollinger, J. M., Jr., and Solomon, E. I. (2004) Electronic and spectroscopic studies of the non-heme reduced binuclear iron sites of two ribonucleotide reductase variants: Comparison to reduced methane monooxygenase and contributions to O_2 reactivity. *J. Am. Chem. Soc. 126*, 3777−3788.
(36) Cryle, M. J., Meinhart, A., and Schlichting, I. (2010) Structural characterization of OxyD, a cytochrome P450 involved in β-hydroxytyrosine formation in vancomycin biosynthesis. *J. Biol. Chem. 285*, 24562−24574.
(37) Stubbe, J., Nocera, D. G., Yee, C. S., and Chang, M. C. Y. (2003) Radical initiation in the class I ribonucleotide reductase: Long-range proton-coupled electron transfer? *Chem. Rev. 103*, 2167−2201.
(38) Muller, J., Lugovskoy, A. A., Wagner, G., and Lippard, S. J. (2002) NMR structure of the [2Fe-2S] ferredoxin domain from soluble methane monooxygenase reductase and interaction with its hydroxylase. *Biochemistry 41*, 42−51.
(39) Sobrado, P., Lyle, K. S., Kaul, S. P., Turco, M. M., Arabshahi, I., Marwah, A., and Fox, B. G. (2006) Identification of the binding region of the [2Fe-2S] ferredoxin in stearoyl-acyl carrier protein desaturase: Insight into the catalytic complex and mechanism of action. *Biochemistry 45*, 4848−4858.
(40) Koglin, A., Mofid, M. R., Löhr, F., Schäfer, B., Rogov, V. V., Blum, M.-M., Mittag, T., Marahiel, M. A., Bernhard, F., and Dötsch, V. (2006) Conformational switches modulate protein interactions in peptide antibiotic synthetases. *Science 312*, 273−276.
(41) Lai, J. R., Koglin, A., and Walsh, C. T. (2006) Carrier protein structure and recognition in polyketide and nonribosomal peptide biosynthesis. *Biochemistry 45*, 14869−14879.
(42) Cryle, M. J., and Schlichting, I. (2008) Structural insights from a P450 carrier protein complex reveal how specificity is achieved in the P450BioI ACP complex. *Proc. Natl. Acad. Sci. U.S.A. 105*, 15696−15701.
(43) Tanovic, A., Samel, S. A., Essen, L.-O., and Marahiel, M. A. (2008) Crystal structure of the termination module of a nonribosomal peptide synthetase. *Science 321*, 659−663.
(44) Farquhar, E. R., Koehntop, K. D., Emerson, J. P., and Que, L., Jr. (2005) Post-translational self-hydroxylation: A probe for oxygen activation mechanisms in non-heme iron enzymes. *Biochem. Biophys. Res. Commun. 338*, 230−239.
(45) Kurtz, D. M., Jr. (2006) Avoiding high-valent iron intermediates: Superoxide reductase and rubrerythrin. *J. Inorg. Biochem. 100*, 679−693.
(46) Froland, W. A., Andersson, K. K., Lee, S.-K., Liu, Y., and Lipscomb, J. D. (1992) Methane monooxygenase component B and reductase alter the regioselectivity of the hydroxylase component-catalyzed reactions. A novel role for protein-protein interactions in an oxygenase mechanism. *J. Biol. Chem. 267*, 17588−17597.
(47) Mitić, N., Schwartz, J. K., Brazeau, B. J., Lipscomb, J. D., and Solomon, E. I. (2008) CD and MCD studies of the effects of component B variant binding on the biferrous active site of methane monooxygenase. *Biochemistry 47*, 8386−8397.
(48) Baker, N. A., Sept, D., Joseph, S., Holst, M. J., and McCammon, J. A. (2001) Electrostatics of nanosystems: Application to microtubules and the ribosome. *Proc. Natl. Acad. Sci. U.S.A. 98*, 10037−10041.